

# Influence of Admixtures of Mineral Elements in Reducing Agents on the Structure of FeSi and FeSiCr Ferroalloys <sup>†</sup>

Wojciech Bialik <sup>1,\*</sup>, Stanisław Gil <sup>1</sup> , Tomasz Pawlik <sup>1</sup>, Sławomir Kozłowski <sup>2</sup>  and Konrad Kołtun <sup>2</sup>

<sup>1</sup> Faculty of Materials Engineering and Metallurgy, Silesian University of Technology, 40-019 Katowice, Poland; stanislaw.gil@polsl.pl (S.G.); tomasz.pawlik@polsl.pl (T.P.)

<sup>2</sup> Re Alloys sp. z o.o., 43-170 Łaziska Górne, Poland; slawomir.kozlowski@realloys.pl (S.K.); konrad.koltun@realloys.pl (K.K.)

\* Correspondence: wojciech.bialik@polsl.pl

<sup>†</sup> Presented at the 30th International Conference on Modern Metallurgy—Iron and Steelmaking, Kosice, Slovakia, 27–29 September 2023.

**Abstract:** This publication presents the chemical compositions of carbon reducers used in the production of ferroalloys, with particular emphasis on the content of Al, Ca, Mg, Mn, Cr, Ti, P, or S in their mineral substances. A certain amount of these elements is transferred to the produced alloys, creating inclusions and precipitations in the metal structure. Most of them are undesirable and adversely affect the final effect of the production process. The work includes sample images of the microstructure of alloys, the chemical compositions of the samples at the test point, and diffragrams. On the basis of the obtained metallographic data, technological observations are made, especially of the crushing process and the amount of grain fractions obtained.

**Keywords:** ferrosilicon; submerged arc furnace; casting ladles; improving purity of alloy



**Citation:** Bialik, W.; Gil, S.; Pawlik, T.; Kozłowski, S.; Kołtun, K. Influence of Admixtures of Mineral Elements in Reducing Agents on the Structure of FeSi and FeSiCr Ferroalloys. *Eng. Proc.* **2024**, *64*, 20. <https://doi.org/10.3390/engproc2024064020>

Academic Editors: Branislav Bul'ko, Dana Baricová, Peter Demeter and Róbert Dzurňák

Published: 29 April 2024



**Copyright:** © 2024 by the authors. Licensee MDPI, Basel, Switzerland. This article is an open access article distributed under the terms and conditions of the Creative Commons Attribution (CC BY) license (<https://creativecommons.org/licenses/by/4.0/>).

## 1. Introduction

The quality of raw materials, especially carbon reducers, used in the production of ferroalloys (based on silicon), has a significant impact on the course of the carbothermic reduction of silica and on the quality of the finished alloy and its microstructure. The amount and chemical composition of the mineral substance contained in the reducers introduced with the charge into the working space of the resistance-arc furnace (coke, hard coal, brown coal, wood chips, etc.) may worsen or improve the technological indicators of the process. This applies to the range of unit indicators of electricity and raw material consumption as well as the daily efficiency of the furnace unit, mainly due to the change in the charge resistance and the need to provide additional electric energy and coal to reduce ash oxides [1–4]. The amount and chemical composition of ash also determine the chemical composition of the finished alloy, especially in terms of the content of undesirable elements, such as phosphorus, titanium, or aluminum, which largely pass into the ferroalloy and contaminate it [5–8]. In addition, phosphorus and aluminum form low-melting eutectic phases, the presence of which leads to the self-decomposition of ingots of silicon alloys [9–11].

## 2. Materials and Experimental Works

The analysis of the impact of the raw materials used, especially carbon reducers, on the composition of the obtained products was carried out for 12 ferroalloys. They were produced on an industrial scale in large quantities. During production, efforts were made to obtain an appropriate number of samples with an average composition. This paper presents the results obtained for 2 alloys (A and B) selected from 12 ferroalloys. They differ in the content of chromium in the alloy. In the technological process, quartzite containing 98.5% SiO<sub>2</sub>, 0.5–0.7% Al<sub>2</sub>O<sub>3</sub> and trace amounts of TiO<sub>2</sub> and CaCO<sub>3</sub> was used as a silicon-supplying raw material. Mixtures of hard coals with the addition of wood chips were

used as a reducer in the process. During the production of alloy A, Colombia coal, with the addition of wood chips, was used as a reducing agent. In the production of alloy B, a mixture of coals was used: 60% Staszic coal and 40% Kazakhstan coal supplemented with wood chips. Table 1 presents the basic properties of carbon reducers included in the material and energy balances of the ferroalloy smelting process, where (as received):  $W^r$ —moisture,  $A^r$ —ash,  $V^r$ —volatile matter,  $C_{fix}$ —hard carbon content,  $Q_i^r$ —heating value. The primary task of the reducer is to supply the appropriate amount of carbon ( $C_{fix}$ ) to the process in accordance with the stoichiometry of the silica reduction reaction. Other properties are also important, such as reactivity to  $SiO(g)$ , particle size distribution, stability of chemical composition, and physical properties (resistivity). The data presented in Table 1 shows a large variation in the properties of the tested reducers. This applies in particular to the carbon content of  $C_{fix}$  and the content of volatile matter.

**Table 1.** Basic properties of carbon reducers.

Reducer	$W^r$	$A^r$	$V^r$	$C_{fix}$	$Q_i^r$
	wt. %				MJ/kg
Staszic coal	4.7	3.3	30.48	61.52	30.718
Colombia coal	12.4	3.5	35.03	49.07	25.636
Kazakhstan coal	11.7	4.2	36.57	47.53	25.013
Wood chips	40.5	0.5	49.32	9.68	10.101

In the obtained metal, inclusions are affected by the components contained in the mineral residue of reducers. Table 2 shows the average composition of the mineral substances of the reducers.

**Table 2.** The average composition of the mineral substances of the reducers.

Chemical Composition of Ash	Reducer			
	Staszic Coal	Colombia Coal	Kazakhstan Coal	Wood Chips
$SiO_2$	14.48	46.2	52.1	44.13
$Al_2O_3$	12.68	17.99	25.39	4.21
$Fe_2O_3$	31.04	8.43	3.63	3.35
CaO	11.32	6.18	3.02	16.88
MgO	7.96	2.21	1.44	3.64
$Na_2O$ wt. %	2.44	4.27	1.56	1.12
$K_2O$	0.61	0.91	0.6	6.31
$SO_3$	12.08	6.5	1.32	1.66
$TiO_2$	0.31	0.78	1.41	0.37
$P_2O_5$	0.62	0.16	2.12	1.99
$Mn_3O_4$	0.53	0.07	0.08	2.64

In the production of alloy A, it was necessary to introduce a chromium carrier into the working space of the furnace (in the traditional process, ores containing chromium are used). To produce alloy A, high-carbon ferrochrome was used, the chemical composition of which is shown in Table 3.

**Table 3.** Chemical composition of high-carbon ferrochrome.

Component	Cr	Si	Fe	Mn	P	Al	C	S
Contents, wt. %	63.68	0.94	25.16	0.103	0.019	0.019	9.11	0.030

### 3. Results

The obtained alloy A was characterized by a minimum content of 60% Si and 20% Cr and was commercially marked as FeSi<sub>60</sub>Cr<sub>20</sub>. Its characteristic feature is a very low carbon content, which has been achieved at the level of 0.025%. Alloy B is a traditional FeSi<sub>65</sub> with a reduced titanium content, the content of which is three times less than allowed by the ISO 5445 standard [12]. The alloy compositions were obtained thanks to a rigorous selection of raw materials and a special modification of the production process. One of the ways to reduce the non-metallic inclusion content of liquid metal is by refining it in a ladle through technical gas purging. Gas bubbles, moving to the liquid metal surface, facilitate the flow of non-metallic inclusions. Depending on the type of process, refining gases can be inert gases or their mixtures with other gases as well as nitrogen, oxygen, air, or oxygen-enriched air. The microstructures of the tested alloys are shown in Figure 1.

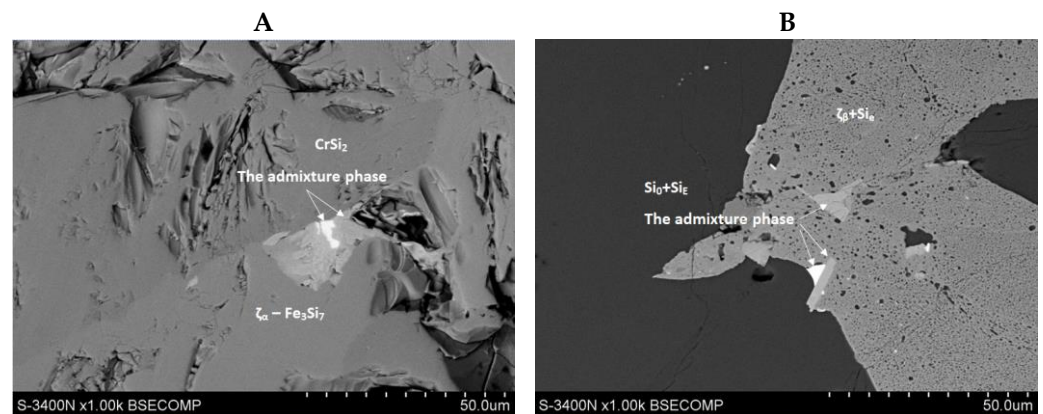


**Figure 1.** The microstructure of the samples observed in a scanning microscope using BSE imaging at 1000× magnification: (A) in the triple eutectic region CrSi<sub>2</sub> + Si + Fe<sub>3</sub>Si<sub>7</sub> (numerous cracks and phases are also visible), (B) in the area of the leboite phase, products of eutectoid transformation are visible—ζ<sub>β</sub> + Si<sub>E</sub>.

For alloy A, an image of the structure is shown at 1000× magnification from the space between the CrSi<sub>2</sub> and Si phases (triple eutectic region). The ζ<sub>α</sub> phase could be distinguished in the image. The Fe<sub>3</sub>Si<sub>7</sub> phase in its image gives a slightly lighter shade of gray than the CrSi<sub>2</sub> phase, mainly due to the presence of iron in the leboite phase, which in turn does not occur in CrSi<sub>2</sub>. For alloy B, the image shows the contrast between the two basic components of the Fe-Si type alloy, i.e., leboite phase ζ (bright areas) and Si + Si<sub>E</sub> silicon crystals (dark areas). In addition, oxide inclusions (black areas) were observed in the image. Microstructure observations within the microareas located along the ζ/Si interface showed that the observed leboite phase was a low-temperature ζ<sub>β</sub> variant with constant FeSi<sub>2</sub> stoichiometry, accompanied by an additional decomposition product of the high-temperature phase—eutectoid silicon Si<sub>E</sub> with the size of individual crystallites reaching several μm—Figure 1B. The triple eutectic microarea at the CrSi<sub>2</sub> and Si phase interface for alloy A is shown in Figure 2A, and the chemical composition at the tested points is shown in Table 4.

**Table 4.** Chemical compositions of sample A at the tested points, %<sub>at</sub>.

Point	Al	Si	Ca	Ti	Cr	Mn	Fe	Ni	Zr
1	–	49.65	–	–	49.09	–	–	–	–
2	–	100	–	–	–	–	–	–	–
3	5.86	34.29	5.80	–	1.82	–	11.68	39.92	–
4	2.89	38.58	–	11.14	–	–	29.72	7.93	7.85

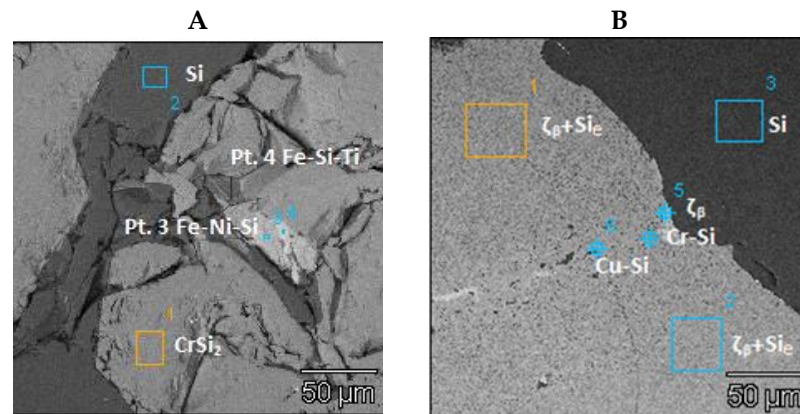


**Figure 2.** The microarea of the samples observed in the scanning microscope: (A) triple eutectic microarea at the phase separation boundary  $\text{CrSi}_2$  and Si, (B) microregion of the  $\zeta$  phase along the boundaries of the  $\zeta/\text{Si}$  interface (brighter inclusions of foreign phases are visible, as are eutectoid decomposition products of the high-temperature  $\zeta_\alpha$  phase into the  $\zeta_\beta$  phase and eutectoid silicon  $\text{Si}_e$ ).

For alloy B, the microregion of the  $\zeta$  phase along the  $\zeta/\text{Si}$  interface, as well as the eutectoid decomposition products of the high-temperature  $\zeta_\alpha$  phase to the  $\zeta_\beta$  phase and eutectoid silicon  $\text{Si}_e$  are shown in Figure 2B. The chemical composition at the tested points of alloy B is presented in Table 5. Additionally, Figure 2A,B show the elements Mn, Ti, Ni, Cr, and Cu, which were introduced with the charge materials. Titanium was introduced with quartzites and the mineral residues of the reducers, while manganese was introduced with coal from the Staszic Mine and with wood chips and steel shavings. The steel shavings also contained trace amounts of nickel, chromium, and copper. The measurements showed that some of these additives are located in the interdendritic space of the alloy.

**Table 5.** Chemical compositions of sample B at the tested points, %<sub>at.</sub>

Point	Al	Si	Ca	Ti	Cr	Mn	Fe	Ni	Zr
1	–	56.53	–	–	–	43.47	–	–	–
2	–	56.21	–	–	–	43.79	–	–	–
3	–	100	–	–	–	–	–	–	–
4	2.77	47.43	–	10.15	36.43	3.22	–	–	–
5	3.45	46.69	–	–	–	42.13	–	–	6.98
6	4.81	29.10	5.54	–	–	9.08	1.29	40.09	–

The results obtained by XRD analysis show that the microstructure of sample A consists of the following phases: regular Si phase, hexagonal  $\text{CrSi}_2$  phase, and tetragonal  $\zeta_\alpha\text{-Fe}_3\text{Si}_7$  phase. The observed structure is partially compatible with the phase equilibrium system in the Fe-Si-Cr system and the literature [13]. The incompatibility is related to the observation of the high-temperature phase  $\zeta_\alpha$ . It seems that for the crystallization and cooling of the crystallized alloy in industrial conditions, there are no conditions for eutectoid decomposition of the  $\text{Fe}_3\text{Si}_7$  phase to  $\text{FeSi}_2$ , Si, and  $\text{CrSi}_2$ . No disintegration was also noted when inspecting the microstructure using a scanning microscope (Figure 1A). Potential decay products, i.e., a mixture of fine precipitates of  $\text{FeSi}_2$ , Si, and  $\text{CrSi}_2$ , were not observed. In conclusion, the  $\text{Fe}_3\text{Si}_7$  phase is a metastable phase of the alloy represented by sample A. The test results for sample B indicate that the main structural components present in the material were Si,  $\zeta_\beta$ , and  $\zeta_\alpha$ . The  $\zeta_\alpha$  phase could not be observed when inspecting the structure using a scanning microscope. The eutectoid decomposition was not complete in the sample volume, and there were places in its volume where the high-temperature leboite variety remained in the form of a residual phase. The structure of sample B is more similar to the equilibrium conditions, which are related to slower crystallization and cooling of the alloy. In addition, it is indicated that microcracks in the sample are incidental,

so the eutectoid transformation is not a factor in determining the tendency of the alloy for self-destruction, which is consistent with the observations in the literature [14].

#### 4. Conclusions

1. The microstructure of sample A, consisting of the phases: regular Si phase, hexagonal  $\text{CrSi}_2$  phase, and tetragonal  $\zeta\alpha\text{-Fe}_3\text{Si}_7$  phase, is partially consistent with the phase equilibrium system in the Fe-Si-Cr system and the literature [13], while the discrepancy is related to the observation of the high-temperature  $\zeta\alpha$  phase. The  $\text{Fe}_3\text{Si}_7$  phase is a metastable phase of the alloy represented by sample A.
2. The main structural components of sample B present in the material were Si,  $\zeta\beta$ , and  $\zeta\alpha$ . There were places in the sample where the high-temperature variety of leboite remained in the form of a residual phase. The structure of the sample is closer to the equilibrium conditions, which is related to the slower crystallization and cooling of the alloy.
3. Microcracks in sample B are incidental, so the eutectoid transformation is not a factor determining the tendency of the alloy to self-destruct, which is consistent with the observations in the literature [14].
4. Elements from mineral additives and iron-bearing materials (scale and steel chips) are located in the interdendritic space of the tested alloys.

**Author Contributions:** Conceptualization, W.B. and S.K.; methodology, S.G.; validation, W.B.; investigation, T.P. and K.K.; writing—original draft preparation, W.B.; writing—review and editing, S.G. and S.K.; supervision, W.B. All authors have read and agreed to the published version of the manuscript.

**Funding:** This paper was partially created with the financial support of Polish Ministry for Science and Higher Education under internal grant BK221/RM0/2018 for Faculty of Materials Engineering and Metallurgy, Silesian University of Technology, Poland.

**Institutional Review Board Statement:** Not applicable.

**Informed Consent Statement:** Not applicable.

**Data Availability Statement:** Data are available in this manuscript.

**Conflicts of Interest:** Authors S.K. and K.K. were employed by the company Re Alloys. The remaining authors declare that the research was conducted in the absence of any commercial or financial relationships that could be construed as a potential conflict of interest.

#### References

1. Machulec, B.; Gil, S.; Bialik, W.; Kozłowski, S. Production of ultrapure ferrosilicon chrome with controlled contents of carbon and other chemical elements for manufacturing of innovative metallic materials. In Proceedings of the METAL 2019—28th International Conference on Metallurgy and Materials, Brno, Czech Republic, 22–24 May 2019.
2. Bialik, W.; Gil, S.; Machulec, B. Physicochemical parameters of carbon reducers for the ferrosilicon smelting process. In Proceedings of the METAL 2018—27th International Conference on Metallurgy and Materials, Brno, Czech Republic, 23–25 May 2018.
3. Ulyeva, G.A. Production of Special Coke for Electrofurnace Production of High-Silicon Alloys. *Coke Chem.* **2022**, *65*, 595–601. [[CrossRef](#)]
4. Strakhov, V.M.; Kashlev, I.M.; Soloviev, M.A. Value of Poorly Caking Coal as a Reducing Agent in Ferrosilicon Production. *Coke Chem.* **2023**, *66*, 63–69. [[CrossRef](#)]
5. Raanes, O.; Kolbeinsen, L.; Byberg, J.A. Statistical analysis of properties for coals used in the production of silicon rich alloys. In Proceedings of the INFACON 8, Beijing, China, 7–10 June 1998.
6. Raanes, O.; Gray, R.J. Coal in the production of silicon rich ferroalloys. In Proceedings of the INFACON 7, Trondheim, Norway, 11–14 June 1995.
7. Schei, A.; Tuset, J.K.; Tveit, H. *Production of High Silicon Alloys*; Tapir Forlag: Trondheim, Norway, 1998.
8. Gasik, M.; Dashevskii, V.; Bizhanov, A. *Ferroalloys. Theory and Practice*; Springer Nature: Cham, Switzerland, 2020.
9. Zubov, V.I.; Gasik, M.I. *Elektrometallurgy of Ferrosilicon. Physical-Chemistry and Technology*; Sistemniye tekhnologii: Dnepropetrovsk, Ukraine, 2002.

10. Zakharov, R.; Petrova, S.; Zhdanov, A.; Zhuchkov, V. Effect of the Structure of Ferrosilicon on Its Desintegration. *Russian Metall. (Met.)* **2014**, *1*, 8–13. [[CrossRef](#)]
11. Broggi, A.; Tveit, H. Growth of impurity phases below the melting point of silicon and consequences on fluidized bed reactor efficiency. In Proceedings of the Silicon for the Chemical and Solar Industry XIII, Kristiansand, Norway, 13–16 June 2016.
12. *ISO 5445:1980*; Ferrosilicon—Specification and Conditions of Delivery. International Organization for Standardization: Geneva, Switzerland, 1980.
13. Li, Z.; Zhou, Z.; Wang, X. Experimental study of the phase relations in the Fe-Cr-Si ternary system at 700 °C. *Int. J. Mater. Res.* **2014**, *105*, 840–846. [[CrossRef](#)]
14. Horn, Q.C.; Heckel, R.W.; Nassaralla, C.L. Reactive phosphide inclusions in commercial ferrosilicon. *Metall. Mater. Trans.* **1998**, *B29*, 325–329. [[CrossRef](#)]

**Disclaimer/Publisher’s Note:** The statements, opinions and data contained in all publications are solely those of the individual author(s) and contributor(s) and not of MDPI and/or the editor(s). MDPI and/or the editor(s) disclaim responsibility for any injury to people or property resulting from any ideas, methods, instructions or products referred to in the content.